UCSF
UC San Francisco Electronic Theses and Dissertations

Title

Evaluation of the feasibility of in vivo Ac-225 imaging

Permalink

https://escholarship.org/uc/item/2pv5d3xm

Author

Du, Shixian

Publication Date

2023

Peer reviewed|Thesis/dissertation

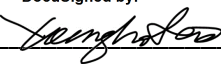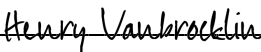Evaluation of the Feasibility of In Vivo Ac-225 Imaging

by
Shixian Du

THESIS
Submitted in partial satisfaction of the requirements for degree of
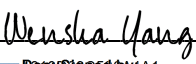MASTER OF SCIENCE

in

Biomedical Imaging

in the

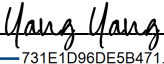GRADUATE DIVISION
of the
UNIVERSITY OF CALIFORNIA, SAN FRANCISCO

Approved:

_____   Youngho Seo

                                                                            Chair

_____   Henry Vanbrocklin

_____   Wensha Yang

_____   Yang Yang

_____

                                                                    Committee Members

II

Acknowledgement

Evaluation of the Feasibility of In Vivo Ac-225 Imaging

Shixian Du

Abstract

Targeted alpha therapy (TAT) is showing promise in the treatment of solid and liquid tumors. TAT uses alpha particles that have small effective range and high linear energy transfer (LET) to achieve high killing in tumor cells and spare normal tissues around the tumor cells. Currently, Actinium-225 (Ac-225) is the most sought-after alpha-emitter. To study the biodistribution of any Ac-225 labeled radiopharmaceuticals, we need to image Ac-225 *in vivo* in small animals at a sub-µCi activity level. With this research question, we investigate the feasibility of using a commercial preclinical single photon emission computed tomography scanner (SPECT) to quantitatively image a mouse-like phantom at low Ac-225 activity. We first developed an Ac-225 imaging protocol with the SPECT scanner. The protocol consisted of calibrating the scanner for two imageable photon emissions from the Ac-225 decay to Fr-221 and Bi-213 (218 keV and 440 keV). Then, we selected regions of interests (ROIs) from phantom images and characterized the quantitative accuracy of the resulting images as a function of activity in µCi equivalent to 1-hour exposure. For both energy windows, with three ROI methods, the recovery coefficients (RCs) showed consistent quantitative accuracy of SPECT images at an activity level as low as 3.36 µCi with 1-hour exposure. 20% or more deviation of RCs from the ground truth as well as increasing variations of RC values measured between phantom cavities were found at activities below 3.36 µCi. Additional phantom studies, at lower activity levels, and animal studies are being prepared for further investigation on the preclinical scanner's limit of detection of Ac-225.

Table of Contents

List of Figures

List of Abbreviations

Ac-225   actinium-225

Bi-213   bismuth-213

Bq (MBq, etc)   becquerel (megabecquerel, etc)

BR   bias ratio

CF   calibration factor

Ci (μCi, etc)   curie (microcurie, etc)

CT   computed tomography

DNA   deoxyribonucleic acid

DSB   double strand break

EDTA   ethylenediaminetetraacetic acid

eV (keV, etc)   electronvolt (kiloelectronvolt, etc)

FOV   field of view

Fr-221   francium-221

LET   linear energy transfer

NaI   sodium iodide

RC   recovery coefficient

ROI   region of interest

SNR   signal-to-noise ratio

SPECT   single photon emission computed tomography

TAT   targeted alpha therapy

VECTor4CT (VECTor)   versatile emission computed tomography (brand name)

1   Introduction

Developing TAT Ac-225 labeled radiopharmaceuticals requires knowledge of the drug biodistribution, which is often determined by *in vivo* and *ex vivo* imaging studies of small animals. In vivo imaging is favored over ex vivo as the former provides a three-dimensional dose map and allows longitudinal studies [1]. However, it has been challenging for researchers to determine Ac-225 activity level, if injected *in vivo*, that will be sufficient for quantitative imaging but low enough to prevent toxicity in small animals such as mice.

1.1   Targeted Alpha Therapy

The TAT therapeutic agents consist of an alpha-emitting radionuclide and stable chelators that also binds to vectors targeting tumor-specific functional groups such as antibodies, peptides, and small molecules [2-3]. In other words, TAT applies the targeted delivery of an alpha-emitter to treat cancer. The high LET radiation from alpha particles primarily targets DNA inside the cancer cell nuclei and causes DNA double strand breaks (DSB) [4-5]. DSB is one kind of radiation-induced DNA damage that is more lethal and difficult to repair, and therefore DSB is considered as the major mechanism of cancer cell death [6]. In summary, the advantageous high LET and small radiation range of alpha-emitting radionuclide result in higher killing in tumor cells and better sparing of surrounding normal tissue cells [7-8].

1.2   Gamma-ray Imaging of Ac-225

Ac-225 is a very promising and popular alpha-emitting radionuclide in targeted alpha therapy (TAT) [4, 8-9]. Ac-225 has a physical half-life of 9.92 days [10]. As Ac-225 decays, shown in

Figure 1, its progeny Fr-221 and Bi-213 emitted photons at 218 and 440 keV, correspondingly. The photon emissions can be detected using SPECT, but the low activities injected *in vivo* makes this imaging technique very challenging in practice.
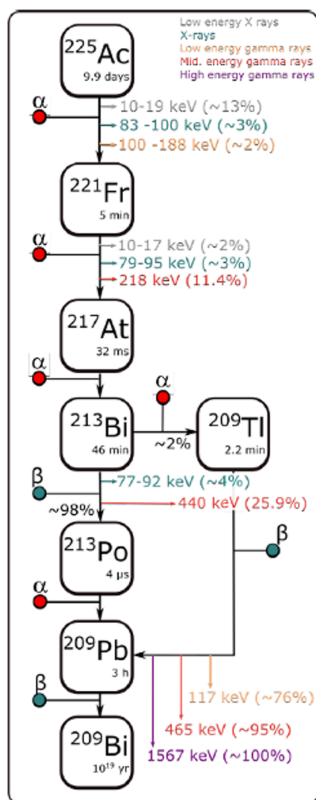
Figure 1: Ac-225 decay chain

Researchers reported de-chelation when injecting Ac-225 *in vivo*, and different chelators showed different chelating stability with Ac-225 [8, 11]. The nucleus recoil after an alpha decay results in chelate instability and release of daughter radionuclide off-target [12]. The accumulation of Bi-213, the progeny of Ac-225, was proved to be cytotoxic to organs such as the kidney in mice. Therefore, research about TAT radiopharmaceuticals needs more information about Ac-225 biodistribution, and there is a need for a method of *in vivo* quantitative Ac-225 imaging.

2   Methods

With a in-house preclinical SPECT/CT scanner (VECTor4CT), the goal is to investigate whether it is possible to quantitatively image Ac-225 at low activities in mouse models. To answer the study question, a vial of Ac-225 in water was prepared and used for protocol development and calibration of Ac-225 imaging with VECTor. Imaging a phantom in the shape and size of a mouse then provided SPECT data for image quality assessment and image analysis by quantification of Ac-225 activity.

2.1   SPECT/CT Instrumentation

The preclinical SPECT/CT scanner (VECTor4CT, MILabs), **as shown in Figure 2(a)**, is located at the imaging suite in UCSF China Basin Landing. The scanner is capable of SPECT/CT multimodality imaging for many radiotherapy radioisotopes at a wide energy range and sub-mm resolution [13, 14]. The scanner is equipped with three heads of detector, each houses a NaI crystal of 9 mm thickness that determines the system sensitivity [14].

Figure 2(b) displayed the collimator chosen for vial and later phantom imaging. The collimator is a multi-pinhole high-energy general-purpose rat and mouse (HE-GP-RM). It has a diameter of 98 mm, and the FOV is 18 mm in axial and 28 mm transverse. A multi-pinhole design improves detection efficiency, and this high-energy collimator has greater septal thickness that detects photons at 440 keV for Bi-213 imaging.
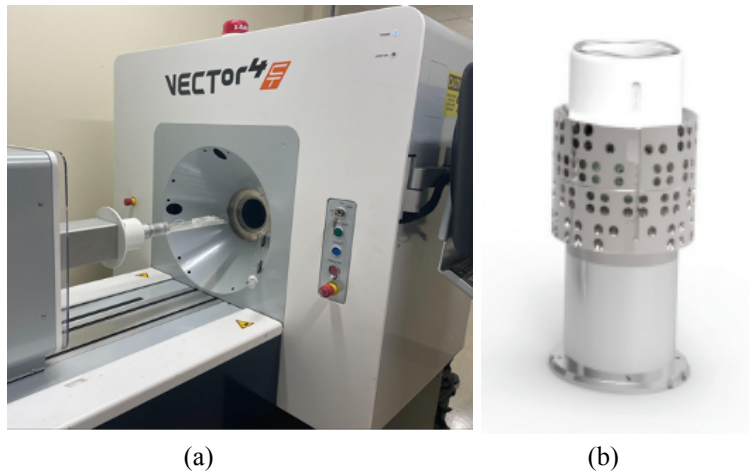
<center>(a)   (b)</center>

Figure 2: The VECTor4CT scanner and collimator HE-GP-RM

2.2   Ac-225 Imaging Protocol

A vial of Ac-225 with an activity of 0.6433 MBq was imaged for Ac-225 image protocol optimization. The energy spectrum of Ac-225 was displayed in **Figure 3** below. The maximums of photopeak were selected at 218 and 440 keV. The widths of the photopeak and background window were determined by optimization of image quality and uniformity, with the latter measuring the ability of the scanner to accurately reproduce the amount of activity within the entire FOV [15].

The uniformity value was calculated from the vial image, as shown in **Figure 4**, as the ratio of standard deviation of the mean activity per voxel and the mean activity per voxel. By optimization, we set the photopeak and background widths to be 25% and 15% of the maximum, respectively. We also found subsets of 4 and 25 iterations to have the better image uniformity and image quality.
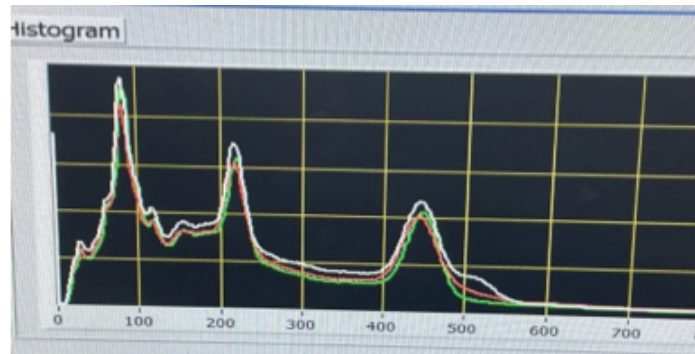
<center>4</center>

Figure 3: The energy spectrum of Ac-225 for image reconstruction
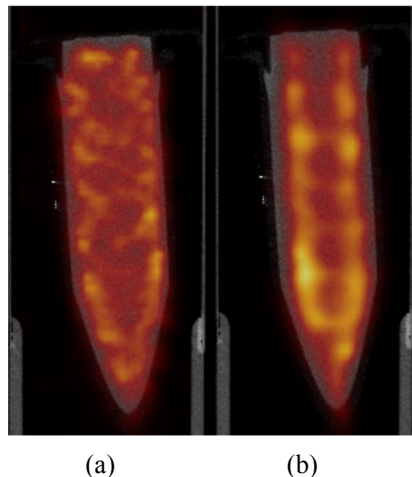

(a)   (b)

Figure 4: SPECT images of calibration vial for (a) Fr-221 and (b) Bi-213

2.3   Calibration of Preclinical SPECT

To calibrate the Ac-225 imaging with VECTor, we need to first determine the true activity and activity concentration inside the calibration vial. The true activity of Ac-225 inside the vial was determined using an automatic gamma counter dedicated to nuclear medicine, which counted gamma emissions with sensitive NaI crystal [16]. The number of gamma counts were obtained in the full energy spectrum of Ac-225, and we converted the gamma counts to activity in Bq with the equation curve pre-calibrated. Since we had the weight of the activity inside vial, we were able to convert the activity then to activity concentration in $\frac{Bq}{mL}$.

Based on the reported activity concentration, physical half-life of Ac-225, and time difference between gamma counting and SPECT imaging, the true activity concentration inside the calibration vial at the time of SPECT imaging can be determined and corrected by decay.

The calibration factor (CF) derived for SPECT imaging will be specific to the choice of radionuclide and collimator. In this case, imaging the calibration vial provided us with CFs for Ac-225 SPECT imaging at 218 keV and 440 keV, corresponding to the Ac-225 progeny Fr-221 and Bi-213. The Fr-221 and Bi-213 images of the calibration vial were shown in **Figure 4(a) and 4(b)**. The CF, as derived in **Eq. 1**, converts counts in image voxels of activity to the total activity inside the vial, and carries a unit of $\frac{Bq}{mL}$.

$$CF_i = \frac{A_{total}(Bq)}{A_{voxel,i} \times N_{voxel} \times V_{voxel}} \qquad \textbf{Eq. 1}$$

2.4   Phantom Preparation and Imaging

The mouse phantom was weighed before and after filling Ac-225 to determine the total volume of Ac-225 inside the phantom. The mouse phantom was filled with 0.4973 MBq Ac-225 in 4.2387 mL and sealed before imaging for 12 hours in the SPECT scanner. Since we extracted the Ac-225 from the calibration vial to fill the phantom, the true activity concentration of the mouse phantom should be equivalent to the true activity concentration inside the calibration vial. The volume of individual cavities of the mouse phantom was also pre-determined by CT image segmentation using ITK-SNAP [17]. Verification of the segmentation volume was done by a water-filling experiment with the phantom and comparison of the water weight at each cavity with the ITK-SNAP statistics.

Based on the information we collected, we applied **Eq. 2** to compute the total activity sealed inside the entire phantom as well as the activity and activity concentration inside the individual cavities of the mouse phantom.

$$A_i = a_{true} \times V_i$$ **Eq. 2**

The mouse phantom would then be fixed to the mouse bed and imaged with CT and SPECT using VECTor. CT is acquired before SPECT for image registration and attenuation correction, both using the vendor-provided software from MILabs. We used the developed imaging protocol for 218 keV and 440 keV to reconstruct images for Fr-221 and Bi-213.

2.5   Image ROI Selection

Regions of interest (ROIs) were selected to quantify activities inside individual cavities of the mouse phantom. We defined three different methods to choose ROIs as shown in **Figure 5**: small, large, and mask ROIs. This approach allowed us to compare which ROI method would perform the best in the quantification of activity in Ac-225 imaging.

The small and large ROIs were manually selected and analyzed with the software Amide [18]. The mask ROIs were identified from the empty phantom CT images using a semi-automatic segmentation implemented in the software ITK-SNAP [17]. Then the segmentation file would be imported to scripts we developed in MATLAB for quantification analysis.
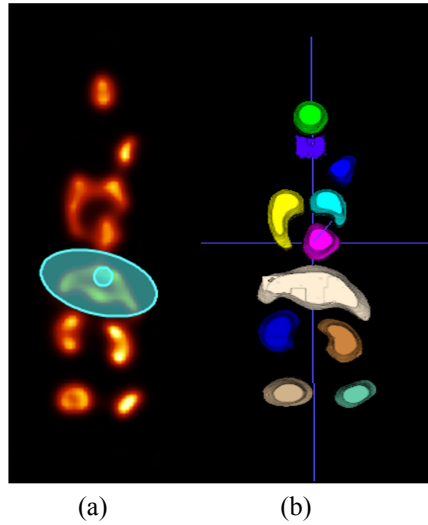
Figure 5: ROIs at mouse phantom images, (a) small/large and (b) mask methods

2.6 Quantification of Activity

We computed the total activity in each ROI by multiplying the mean activity per voxel by the voxel size and total number of voxels selected by the ROI. The computed total activity was previously calibrated using the CFs derived from **Eq. 1**. Next, with the known volume of ROI obtained from image segmentation, we would calculate a measured activity concentration. The measured activity concentration was then compared with true activity concentration as determined by the gamma counter and corrected by decay.

In summary, we collected three sets of activity measurements corresponding to three ROI methods per energy window. In addition, we repeated the steps for both energy windows, Fr-221 and Bi-213. In total, there would be six sets of quantification data for Ac-225 SPECT imaging with the VECTor scanner.

8

For each dataset, we calculated recovery coefficients (RC). RC is the ratio of measured and true activity concentration per cavity, as shown in **Eq. 3**. Therefore, a RC value very close to 1 means little deviation from the ground truth and good signal recovery by the scanner.

$$RC_i = \frac{a_{measured}}{a_{true}} \qquad\qquad \textbf{Eq. 3}$$

Similarly, for each dataset, we calculated the deviation from 12-hour imaging, named as BR or bias ratio. BR is defined as the ratio of measured activity concentration at lower activities to measured activity concentration at full activity, as indicated in **Eq. 4**. The full activity was 0.4973 MBq (13.44 µCi) or 161.09 µCi equivalent for one-hour imaging. The SPECT images of lower activities were emulated by reducing counts in image reconstruction.

$$BR_i = \frac{a_{measured}}{a_{measured-12hr}} \qquad\qquad \textbf{Eq. 4}$$

3   Results

Ac-225 phantom images with full and emulated low activities were obtained from VECTor SPECT imaging and presented in **Figure 6** and **Figure 7**. Count reductions in SPECT image reconstructions were performed to emulate lower activities, which were calculated in proportion to the percentage of count reduced.

In addition, the values of recovery coefficient and bias ratio to 12-hour imaging, for each individual cavity of the mouse phantom, were plotted against the amount of activity in µCi equivalent to 1-hour imaging. The RC and BR plots for each ROI method and for both 218 and 440 keV energy windows were presented in **Figure 8 to Figure 11**. The activity levels on the x-axis of these plots, if converted to those under 1-hour scan time, will give a better estimate of the amount of activity required for small animals *in vivo* imaging.

3.1   Phantom Images

From qualitative assessment of the phantom images, we found that VECTor SPECT imaging was able to resolve all cavities of the mouse phantom, ranging from a volume of 0.1974 mL to 1.193 mL. This is true for both Fr-221 and Bi-213 images. However, the Bi-213 images showed worse image resolution than the Fr-221 images.

The image resolution also degraded with lower activity levels. By the time Ac-225 activity level was lowered to 0.0104 MBq (emulated), not all cavities inside the mouse phantom can be clearly resolved. The SPECT images were unable to distinguish cavities in proximity to each other, such as the left and right lung, as well as the heart below the lungs.
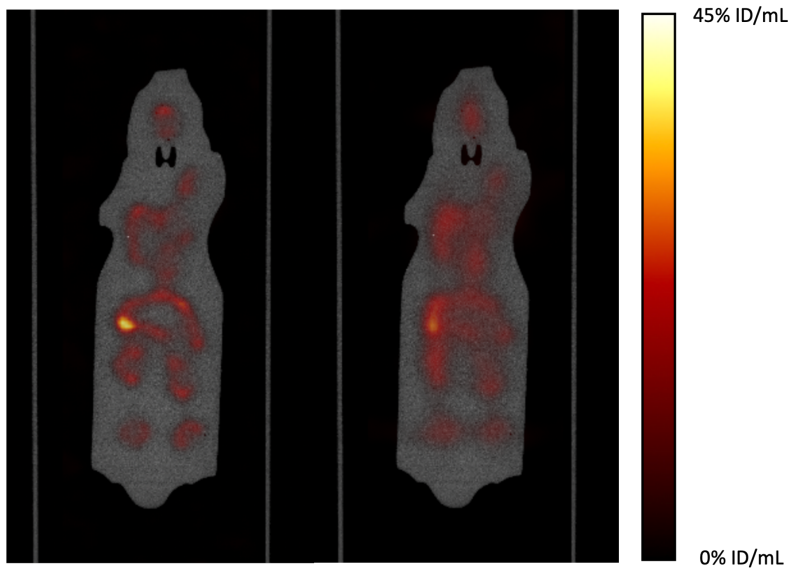
**Figure 6:** Ac-225 images of (a) Fr-221 and (b) Bi-213 with 0.4973 MBq
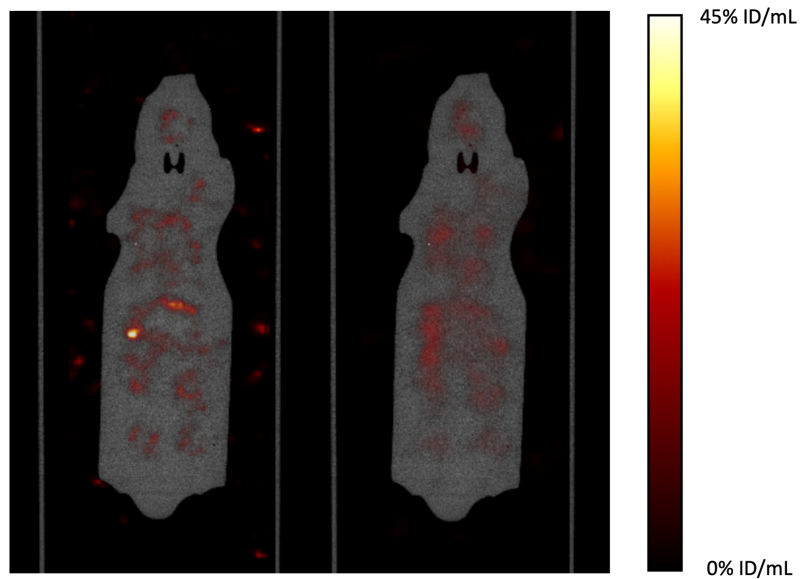
Figure 7: Ac-225 images of (a) Fr-221 and (b) Bi-213 with emulated 0.0104 MBq

3.2 Quantitative Analysis

Both Fr-221 and Bi-213 images were able to demonstrate that RCs, quantified with three ROI methods, remained consistent at an emulated activity as low as 3.36 μCi. Starting at an activity level of 1.68 μCi, we observed fluctuations of RC values. The mask ROI method indicated decreasing RCs in the Fr-221 and Bi-213 images, while the other two ROI methods showed more random fluctuation of RC values.

In addition, as the activity reduced to 1.68 μCi, we found greater variations of RC between different cavities inside the same phantom. The mask ROI method showed least RC variation, while the small ROI method showed greatest amount of RC variation as the activity reached to 1.68 μCi and continued lowering.

For the BR plots, we observed a similar limit of detection. The small ROI plots demonstrated that when the activity was lowered to 3.36 μCi, we started to find a deviation of RC for more than 20% from the 12-hour imaging case. The mask ROI plots provided slightly improved quantification, suggesting a BR of 0.8 at an activity level at 1.68 μCi. The large ROI plots did show smaller deviations but at a BR larger than 1.
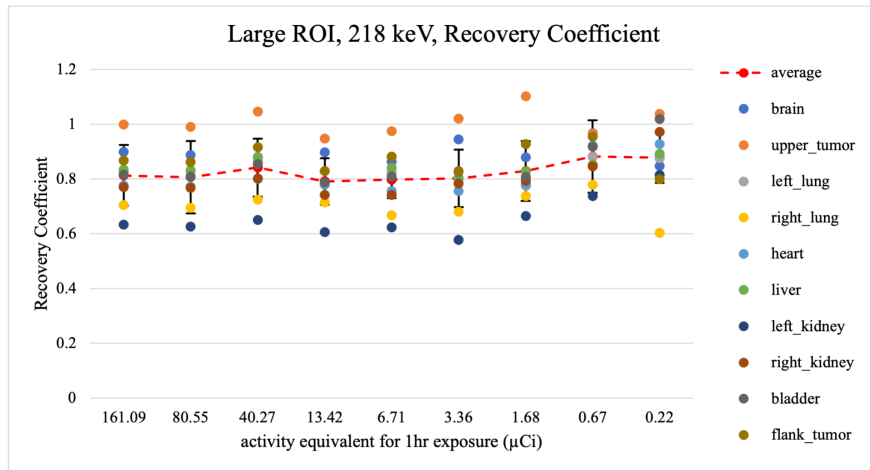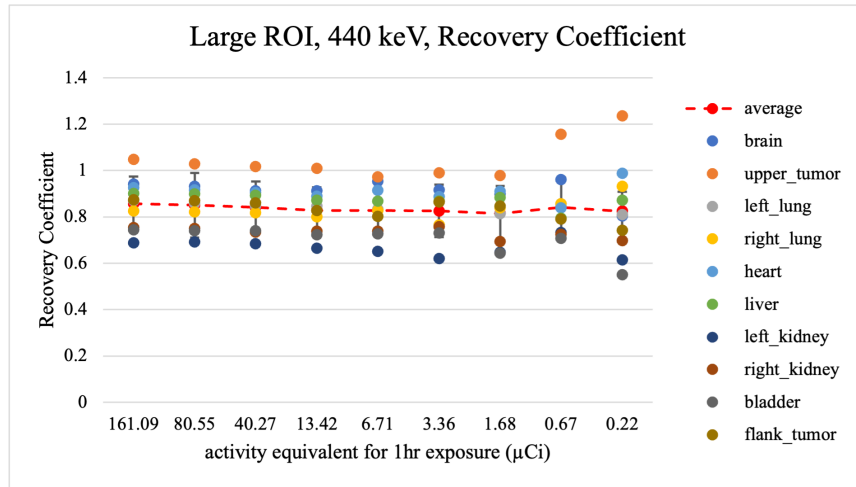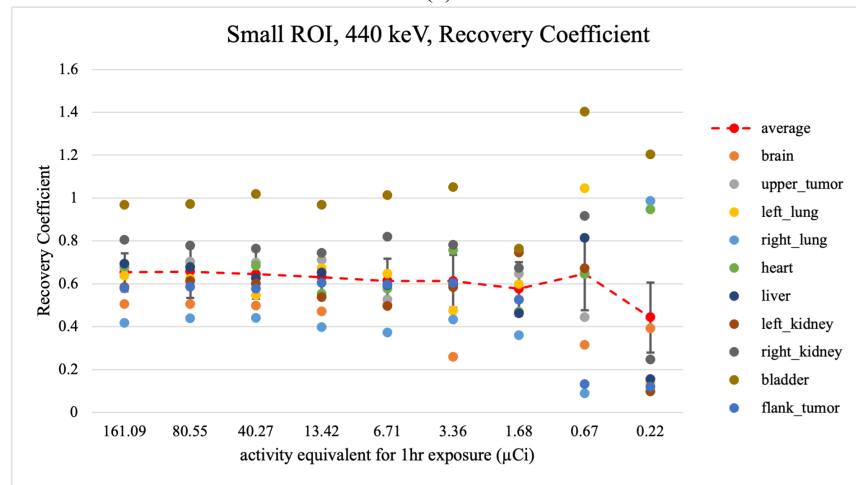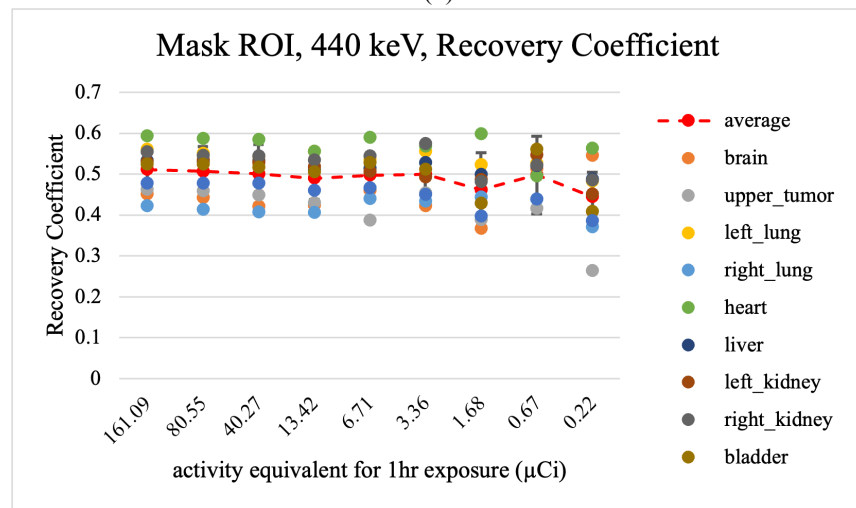
(a)
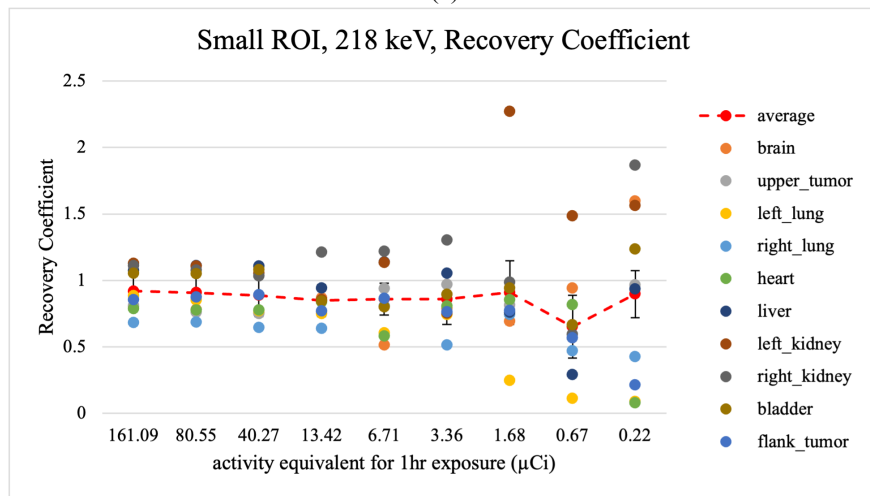
(b)
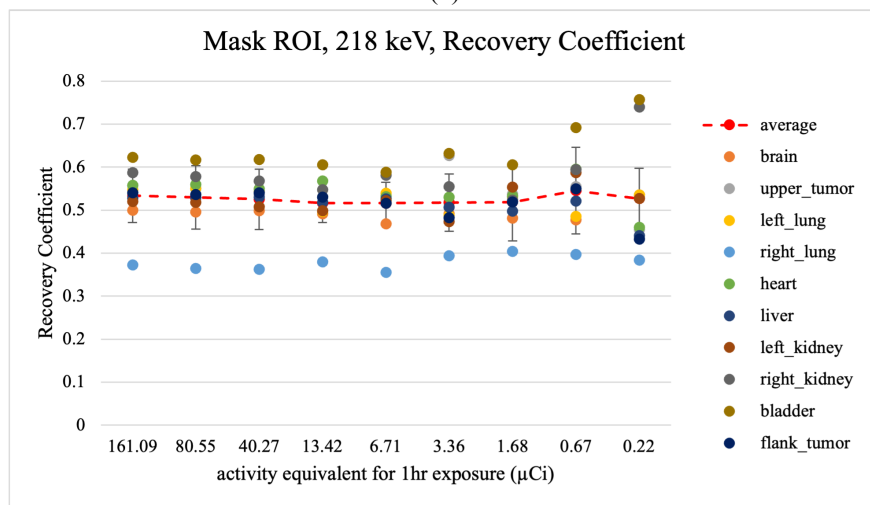
(c)

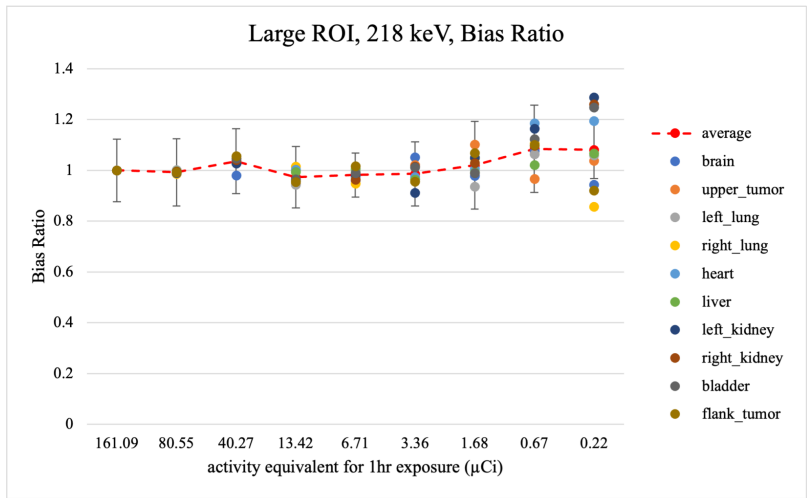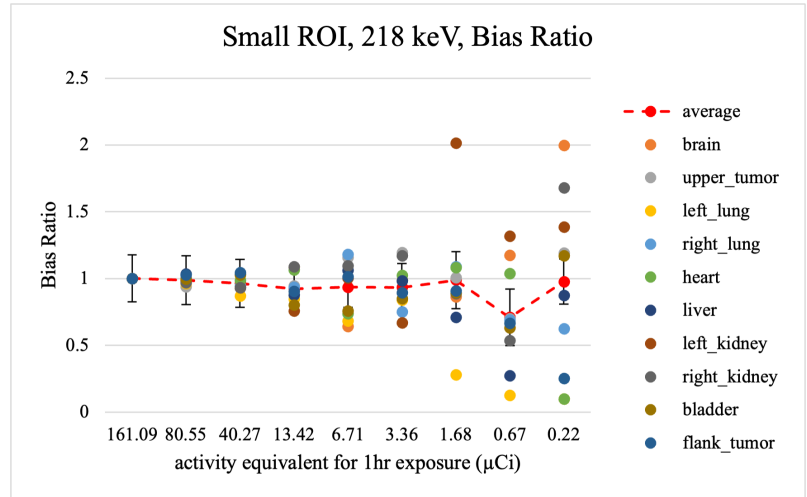**Figure 8:** RCs for Fr-221, (a) large (b) small, and (c) mask ROIs
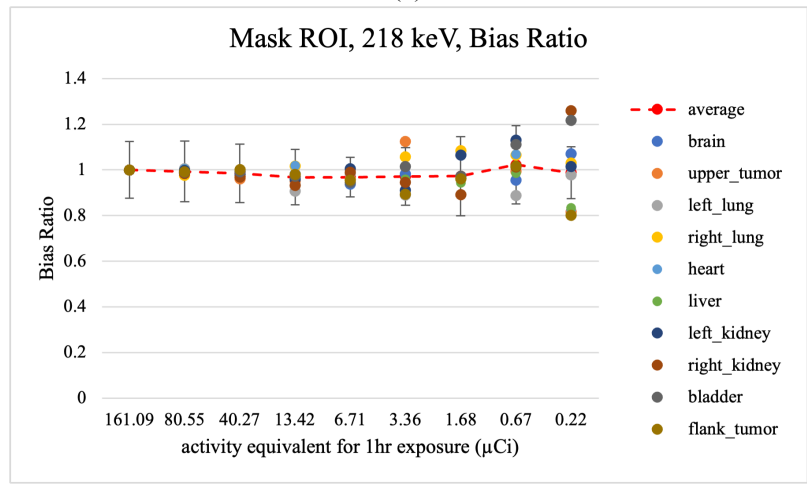
13

(a)

(b)

(c)

Figure 9: RCs for Bi-213, (a) large (b) small, and (c) mask ROIs
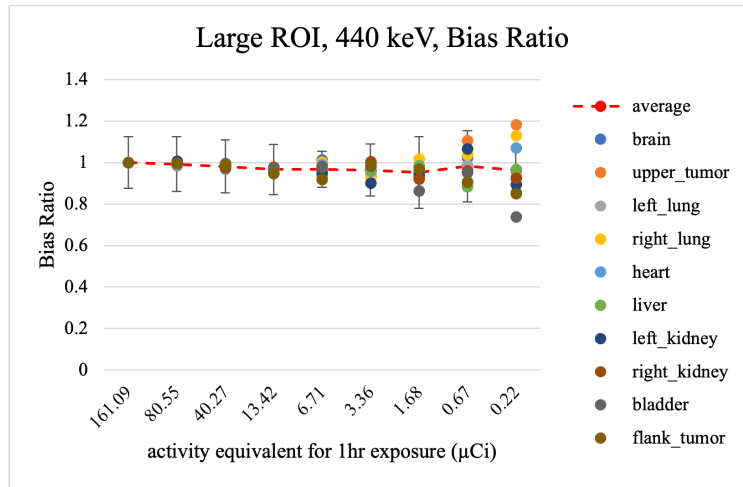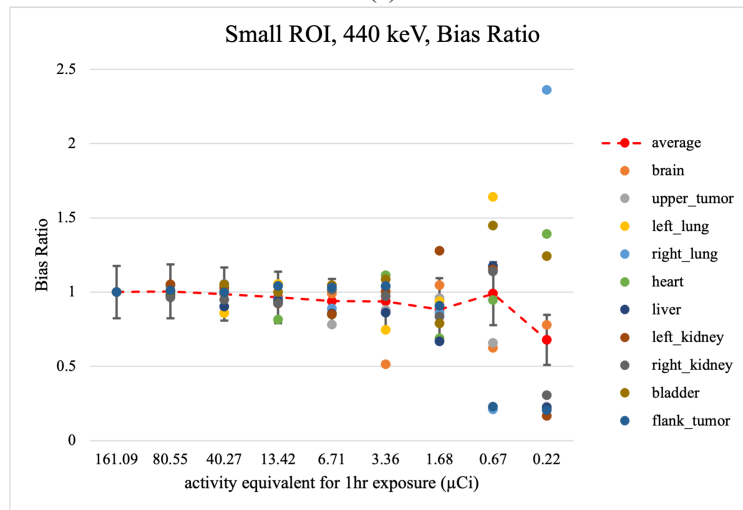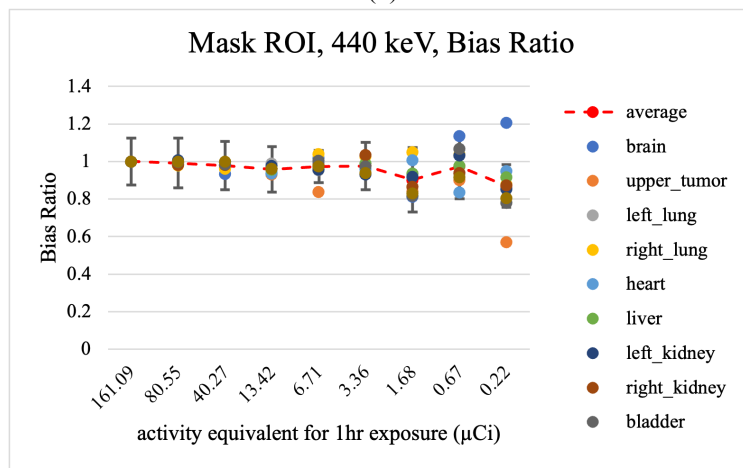
(a)

(b)

(c)

Figure 10: BRs from 12-hr for Fr-221, (a) large (b) small, and (c) mask ROIs

15

(a)

(b)

(c)

Figure 11: BRs from 12-hr for Bi-213, (a) large (b) small, and (c) mask ROIs

16

4   Discussion

The high-energy collimator we currently employ permits Bi-213 imaging, but this comes at the cost of diminished image resolution for Bi-213. The reduced resolution can be attributed to increased septal penetration from the high-energy gamma rays at 440 keV. Addressing this challenge may require the adoption of a specialized high-energy collimator [19]. However, due to the trade-off between spatial resolution and sensitivity in SPECT, using a high-energy collimator would reduce sensitivity, which is crucial for ultra-low activity experiments.

This finding might be able to explain the decreased RCs of Bi-213 images obtained from small ROI methods. The activity and activity concentration values quantified from the images would vary with where the ROI was selected. In the selection of ROIs, we want the ROI to cover the activity of interest only, if possible. However, the number of voxels of activity would depend on the image resolution and factors such as SNR and noise [20].

It is worth noting that, in Fr-221 and Bi-213 images, activity accumulated around the sidewall of the phantom cavities. To reduce the sidewall accumulation effect, Ac-225 can be prepared with chelates such as EDTA [8]. Such non-uniformities might explain the lower recovery coefficients obtained from the mask ROI analysis, as indicated in **Figure 8(c)** and **Figure 9(c)**. The activity and activity concentration values quantified from the SPECT images would be significantly lower when the cavity edges, with the most Ac-225 activity, did not fit properly to the segmentation mask.

There are pros and cons of each ROI method. The small ROIs covered partial volume of the phantom cavity, which added bias to the measurement depending on the location selection of the

ROI. From the RC plots, we found a large variation of measurements between cavities with a small ROI. This finding indicated that images were not uniform, and changing the location of RC or altering the size of ROI could yield better RCs. In addition, it could be due to the fact that some cavities could be better filled than others. To address the problem, we can perform more repeats in measurement and refine our protocols to make sure each cavity was filled properly.

The large ROI method covered more than the entire phantom cavity, which ensured that all activities inside the phantom cavity were included in quantification. However, this method was also limited because ROIs for different cavities could overlap and should be carefully selected.

The mask method was able to create ROIs most similar to the shape and size of the phantom cavities. The resulting ROI sizes had very little difference with the actual volumes needed to fill each cavity of the phantom. However, this method was the most time-consuming method as multiple steps were required to create individual ROIs including thresholding, classification, and 3D segmentation. In addition, the mask method would not be as accurate if, for every repeat experiment, new CTs were not as similar to the original template CT. Re-segmentation should be considered for each repeat to improve quantification accuracy.

We sometimes found a RC value greater than 1 from the SPECT images obtained from the two energy windows. Together with the large variations from small ROI, the two findings suggested that we should take extra steps to add shielding for this experiment design. More shielding should be placed outside the detector, as the small activity we were measuring from the phantom could be impacted by any background activities happening in the imaging suite.

5   Conclusion

We demonstrated that the quantitative accuracy of the Ac-225 SPECT imaging with VECTor was consistent until we reached an activity as low as 3.36 µCi as imaging for 1-hour. The result was obtained with a phantom in the shape and size of a mouse, with individual compartments of filled Ac-225. However, *in vivo* imaging would be more complicated, as blood and activity would circulate across different organs inside the animal, and off-target accumulation after certain imaging time would be cytotoxic to the animal. Therefore, the next steps of this study include to explore different collimators in Ac-225 imaging with VECTor and to perform *in vivo* and *ex vivo* animal experiments with VECTor.

References

[1] J. Caravaca, Y. Huh, G. T. Gullberg, and Y. Seo, "Compton and Proximity Imaging of 225Ac In Vivo With a CZT Gamma Camera: A Proof of Principle With Simulations," *IEEE Trans Radiat Plasma Med Sci*, vol. 6, no. 8, pp. 904–915, Nov. 2022, doi: 10.1109/TRPMS.2022.3166116.

[2] C. Parker *et al.*, "Targeted Alpha Therapy, an Emerging Class of Cancer Agents: A Review," *JAMA Oncology*, vol. 4, no. 12. American Medical Association, pp. 1765–1772, Dec. 01, 2018. doi: 10.1001/jamaoncol.2018.4044.

[3] F. Reissig *et al.*, "Towards targeted alpha therapy with actinium-225: Chelators for mild condition radiolabeling and targeting psma—a proof of concept study," *Cancers (Basel)*, vol. 13, no. 8, Apr. 2021, doi: 10.3390/cancers13081974.

[4] J. L. Hatcher-Lamarre, V. A. Sanders, M. Rahman, C. S. Cutler, and L. C. Francesconi, "Alpha emitting nuclides for targeted therapy," *Nuclear Medicine and Biology*, vol. 92. Elsevier Inc., pp. 228–240, Jan. 01, 2021. doi: 10.1016/j.nucmedbio.2020.08.004.

[5] F. Graf *et al.*, "DNA double strand breaks as predictor of efficacy of the alpha-particle emitter Ac-225 and the electron emitter Lu-177 for somatostatin receptor targeted radiotherapy," *PLoS One*, vol. 9, no. 2, Feb. 2014, doi: 10.1371/journal.pone.0088239.

[6] Ross G M, "Induction of cell death by radiotherapy," 1999. [Online]. Available: http://www.endocrinology.org1351-0088/99/006-041

[7] G. Sgouros *et al.*, "MIRD pamphlet No. 22 (Abridged): Radiobiology and dosimetry of α-particle emitters for targeted radionuclide therapy," *Journal of Nuclear Medicine*, vol. 51, no. 2. pp. 311–328, Feb. 01, 2010. doi: 10.2967/jnumed.108.058651.

[8]   D. A. Scheinberg and M. R. Mcdevit, "Actinium-225 in targeted alpha-particle therapeutic applications," 2011.

[9]   A. Morgenstern, C. Apostolidis, and F. Bruchertseifer, "Supply and Clinical Application of Actinium-225 and Bismuth-213," *Seminars in Nuclear Medicine*, vol. 50, no. 2. W.B. Saunders, pp. 119–123, Mar. 01, 2020. doi: 10.1053/j.semnuclmed.2020.02.003.

[10]   S. Pommé *et al.*, "Measurement of the 225Ac half-life," *Applied Radiation and Isotopes*, vol. 70, no. 11, pp. 2608–2614, Nov. 2012, doi: 10.1016/j.apradiso.2012.07.014.

[11]   A. P. Bidkar *et al.*, "Treatment of Prostate Cancer with CD46-targeted 225Ac Alpha Particle Radioimmunotherapy," *Clin Cancer Res*, vol. 29, no. 10, pp. 1916–1928, May 2023, doi: 10.1158/1078-0432.CCR-22-3291.

[12]   N. A. Thiele and J. J. Wilson, "Actinium-225 for targeted α therapy: Coordination chemistry and current chelation approaches," in *Cancer Biotherapy and Radiopharmaceuticals*, Mary Ann Liebert Inc., Oct. 2018, pp. 336–348. doi: 10.1089/cbr.2018.2494.

[13]   MILabs, "MILabs VECTor: A Powerful Platform for Translational Theranostics Research," 2023. https://www.milabs.com/newsletter/theranostics-nov-2017/ (accessed Aug. 20, 2023).

[14]   M. C. Goorden *et al.*, "VECTor: A preclinical imaging system for simultaneous submillimeter SPECT and PET," *Journal of Nuclear Medicine*, vol. 54, no. 2, pp. 306–312, Feb. 2013, doi: 10.2967/jnumed.112.109538.

[15]   P. Keim, "An Overview of PET Quality Assurance Procedures: Part 1," 1994.

[16]   Hidex Oy, "Hidex Automatic Gamma Counter," 2023. https://hidex.com/products/hidex-automatic-gamma-counter/ (accessed Aug. 23, 2023).

[17] ITK-SNAP, "Tutorial: Getting Started with ITK-SnAP." http://www.itksnap.org/docs/viewtutorial.php (accessed Aug. 21, 2023).

[18] A. M. Loening, "AMIDE: Amide's a Medical Imaging Data Examiner," 2012. https://amide.sourceforge.net/ (accessed Aug. 25, 2023).

[19] K. Van Audenhaege, R. Van Holen, S. Vandenberghe, C. Vanhove, S. D. Metzler, and S. C. Moore, "Review of SPECT collimator selection, optimization, and fabrication for clinical and preclinical imaging," *Medical Physics*, vol. 42, no. 8. AAPM - American Association of Physicists in Medicine, pp. 4796–4813, Aug. 01, 2015. doi: 10.1118/1.4927061.

[20] R. Boellaard, N. C. Krak, O. S. Hoekstra, and A. A. Lammertsma, "Effects of Noise, Image Resolution, and ROI Definition on the Accuracy of Standard Uptake Values: A Simulation Study," 2004.

Publishing Agreement

It is the policy of the University to encourage open access and broad distribution of all theses, dissertations, and manuscripts. The Graduate Division will facilitate the distribution of UCSF theses, dissertations, and manuscripts to the UCSF Library for open access and distribution. UCSF will make such theses, dissertations, and manuscripts accessible to the public and will take reasonable steps to preserve these works in perpetuity.

I hereby grant the non-exclusive, perpetual right to The Regents of the University of California to reproduce, publicly display, distribute, preserve, and publish copies of my thesis, dissertation, or manuscript in any form or media, now existing or later derived, including access online for teaching, research, and public service purposes.

DocuSigned by:

Shixian Du

—2E63E28BDD0C402...

Author Signature

8/26/2023

Date